Materials Science and Engineering C 58 (2016) 160–168

Contents lists available at ScienceDirect

Materials Science and Engineering C

journal homepage: www.elsevier.com/locate/msec

# Electrochemical & osteoblast adhesion study of engineered $TiO_2$ nanotubular surfaces on titanium alloys

Zia Ur Rahman [a], Waseem Haider [a,*], Luis Pompa [b], K.M. Deen [c,d]

[a] School of Engineering and Technology, Central Michigan University, Mt. Pleasant, MI, USA
[b] Department of Mechanical Engineering, University of Texas–Pan American, Edinburg, TX, USA
[c] Department of Metallurgy & Materials Engineering, CEET, University of the Punjab, 54590 Lahore, Pakistan
[d] Department of Materials Engineering, University of British Columbia, Vancouver, BC V6T 1Z4, Canada

ARTICLE INFO

*Article history:*
Received 28 September 2014
Received in revised form 30 May 2015
Accepted 10 July 2015
Available online 7 August 2015

*Keywords:*
Nanotubes
Osteoblast
Electrochemical
Potentiodynamic
Impedance spectroscopy

ABSTRACT

$TiO_2$ nanotubes were grafted on the surface of cpTi, Ti6Al4V and Ti6Al4V-ELI with the aim to provide a new podium for human pre-osteoblast cell (MC3T3) adhesion and proliferation. The surface morphology and chemistry of these alloys were examined with scanning electron microscopy and energy dispersive x-ray spectroscopy. $TiO_2$ nanotubes were further characterized by cyclic potentiodynamic polarization tests and electrochemical impedance spectroscopy. The vertically aligned nanotubes were subjected to pre-osteoblast cell proliferation in order to better understand cell–material interaction. The study demonstrated that these cells interact differently with nanotubes of different titanium alloys. The significant acceleration in the growth rate of pre-osteoblast cell adhesion and proliferation is also witnessed. Additionally, the cytotoxicity of the leached metal ions was evaluated by using a tetrazolium-based bio-assay, MTS. Each group of data was operated for $p < 0.05$, concluded one way ANOVA to investigate the significance difference.



## 1. Introduction

Titanium and their alloys are today's armamentarium for orthopedic, dental and cardiovascular surgeons as these materials are extensively used as implant material [1–4]. In orthopedics, titanium is used as plates, pins, fixing screws for bone fractures. Titanium alloys are also used as various components for total hip prostheses and as femoral and tibia components in total knee arthroplasty [5]. Nitinol (alloy of nickel and titanium) is commonly used in cardiovascular application [6]. Low modulus, good fatigue strength, extraordinary corrosion resistant and suitable biocompatibility make titanium and its alloys suitable for biomedical applications [7].

Occasionally, the traditional titanium implants face many complications such as infections, implant loosening and insignificant host tissue integration, which leads to implant failure [8]. Although many of the outcomes are successful, still there are significant problems with implant loosening and failure. The statistics show that 25% of hip replacement surgeries (about 10–15% of dental implant surgeries) were revised due to previous implant failure [9]. Incomplete osseointegration is one of the major causes of the titanium implant failure and its replacement has poorer outcome which sometimes leads to osteolysis of implant [10].

In order to increase the bioactivity of the implants, surface treatments in the form of coating with bioactive material is carried out. Examples include hydroxyapatite, polymers, calcium phosphate and other techniques of surface modification are applied to make Ti more bioactive [11]. Sporadically, these coatings or modified surfaces are not reliable in the long span and tend to fail by fracture and delamination [12]. The plasma sprayed hydroxyapatite is the common coating on metallic implants but high degree of porosities, poor bond strength, and non uniformity make it unfit for long run [13]. Dip coating, ion sputtering, sol–gel coating and electropolishing are the other techniques used as surface treatments [11,14,15].

Previous studies reveal that mesoscale, microscale and nanoscale patterns on surface topography influences the cell adhesion, proliferation and osseointegration [16–18], which impacts the fabrication of prosthesis and load bearing implants [19]. J. E. Feighan et al. found that the micron and submicron scale surface topographies have a significant effect on long-term biomechanical integrity of bone–implant interface. The micro-roughness of the surface has positive impact on the osseointegration. It also provides great cell adhesion which reduces the micro-motions and improves biomechanical interaction [20].

Hulbert et al. investigate that oxide ceramics with minimum interconnected pore diameter of approximately 100 μm was needed for adequate bone ingrowth. It was thought that smaller pore sizes allowed incomplete mineralization of the infiltrating tissue [21]. R. Zhou et.al (2014) found that the amorphous phase $TiO_2$ nano-crystal composite coatings enhance the cell proliferation and the MC3T3-E1 cells have

* Corresponding author at: School of Engineering and Technology, Central Michigan University, Mt. Pleasant, MI, USA.
*E-mail address:* haide1w@cmich.edu (W. Haider).

http://dx.doi.org/10.1016/j.msec.2015.07.024
0928-4931/

long extensive filopodia on the Ti Nano-crystal composite surface [22]. The way the cell interacts with the surface presenting nanostructure is the same as at the other scale, however, the interface of the cell with the surface has distinct attachment due to the intermediacy of the attached proteins [23].

In order to design better implant materials, it is necessary to understand the bone–material interface [24]. It is generally noticed that the fibrous proteins such as fibronectin and vitronectin play a leading role in adhesion and cell proliferation on the implant surface and osseointegration [25]. The first event, which occurs after the implantation of the biomaterial, is the adsorption of proteins from blood and other tissue fluids [26]. Since the surface properties of implant materials intimately affect the initial protein adsorption from biological fluid and further selective recruitment as well as activation of favorable cell functions, nanoscale surface alteration and surface modifications are the most popular methods [27].

In view of the adequacies in these different surface modification techniques, it is necessary to improve and integrate the interface of the bone and implant surface with the interlocked configuration with much increase in adhesion and less continuous interface on nanoscale level to induce a significant cell proliferation growth. In this work $TiO_2$ nanotubes (TNTs) have been grafted on the bulk surface of cpTi, Ti6Al4V and Ti6Al4V-ELI using a simple anodization process. Our method of anodization for nanotubular structure provides more volume for protein absorption in nanotubes, which will definitely increase the biocompatibility and provide new podium for strong osseointegration.

## 2. Experimental

### 2.1. Sample preparation

cpTi, Ti6Al4V and Ti6Al4V-ELI rods of medical grade were cut with high-speed saw into circular disk samples having 0.2 in. thickness and 0.625 in. diameter. The samples were grinded using silicon carbide grit papers on Buehler® abrasive belt grinder. Grit paper sizes: 180, 240, 320, 400, 600, 800, 1000 and 1200 are used in order to achieve smooth surface finish. Prior to anodization each sample was degreased by sonication in acetone for 5 min followed by deionized water rinse.

### 2.2. Anodization

The optimization of anodizing conditions is already explained by Deen et al. [28]. The electrolyte used for the anodization process was carried in a beaker. 0.25 M ammonium chloride ($NH_4Cl$) was mixed with 0.1 M ammonium di-hydrogen phosphate ($NH_4H_2PO_4$), 95.8 ml ethylene glycol, 2 μl of glycerin and 4 ml of DI-water. Before starting the anodization the pH of the electrolyte was measured by a pH meter. Phosphoric acid ($H_3PO_4$) is added drop by drop to the electrolyte in order to bring its pH between 3 and 4. The average pH of n = 5 is depicted in Fig. 1.

The dried and cleaned sample is connected to the positive terminal of the DC source (American Reliance INC. LPS 304.) while the carbon graphite rod is connected to the negative terminal as cathode. The voltage of 60 V is supplied between the two electrodes and allows the system to anodize for two hours. The same procedure is repeated for each sample and each time fresh electrolyte is used. The schematic representation of the anodization setup is shown in Fig. 2.

### 2.3. Surface morphology and chemistry

The surface morphology and chemistry of each anodized specimen were analyzed using scanning electron microscope (Sigma VP Carl Zeiss, Germany) and energy dispersive x-ray spectrometer, respectively.

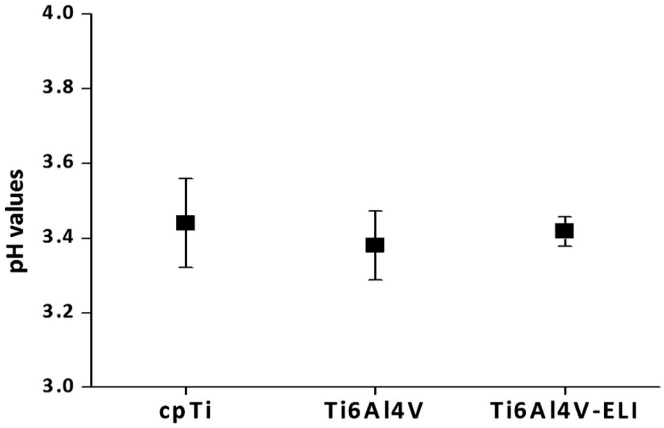


**Fig. 1.** Average pH values of electrolyte for n = 5, used for anodization of respective alloys.

### 2.4. Electrochemical analysis

The electrochemical behavior of nanotubes of cpTi, Ti6Al4V and Ti6Al4V-ELI was studied by performing cyclic potentiodynamic polarization scans and electrochemical impedance spectroscopy (EIS). The conventional three-electrode cell was assembled using saturated calomel electrode (SCE) as reference electrode, carbon graphite as counter electrode and titanium alloy having grafted nanotube sample as working electrode. Both the potentiodynamic scans and EIS were conducted inside the incubator (temperature 37 °C and 5% $CO_2$) by polarizing the sample anodically. The phosphate buffer saline tablets (Part # P4417-50TAB Sigma Aldrich® USA) were used to make phosphate buffer solution by dissolving one tablet in 200 ml of deionized water. This solution is used as an electrolyte. The chemical composition of the electrolyte solution in g/l is mentioned in Table 1.

Gamry potentiostat reference 600 is used for the cyclic potentiodynamic polarization scans and EIS. Gamry framework and Gamry Echem Analyst software are used for data analysis. The scan rate was kept at 1 mV/s and potential range of −500 to 1500 mV against SCE.

In potentiostatic EIS of 10 mV rms, the initial frequency was kept at 300 K-Hz where as final frequency was 0.01-Hz. The area immersed was measured as 1.282 $cm^2$ for each sample in order to get the precise values for each sample.

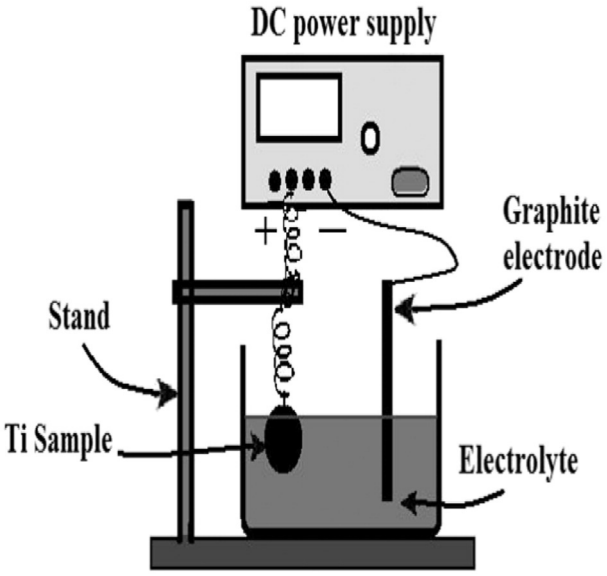


**Fig. 2.** Schematic representation of the anodization setup.

**Table 1**
Chemical composition of PBS solution (g/L).

| NaCl | $Na_2HPO_4$ | $NaHCO_3$ | KCl | $KH_2PO_4$ | $MgSiO_4$ | $CaCl_2$ |
|---|---|---|---|---|---|---|
| 8.0 | 0.06 | 0.35 | 0.4 | 0.06 | 0.2 | 0.14 |

### 2.5. Cell–surface interaction at nanoscale

In order to investigate the effects of nanotubes on pre-osteoblast cells, the surface of each titanium alloy was exposed to these cells. MC3T3-E1 Subclone 4 (ATCC® CRL-2593™) pre-osteoblast cells were grown in a culture flask. After incubation, 90% confluency was achieved and the cells were trypsinized, centrifuged and suspended in culture media for further cell seeding.

The cell culture media was prepared by adding 10% fetal bovine serum (FBS) (Thermo Scientific™ HyClone™ SH3008803HI), 1% Penicillin Streptomycin (Sigma Aldrich P4333) to MEM alpha from (part # SH4007-13, Thermo scientific, USA). The cells were counted by using a hemocytometer and 30,000 cells were allowed to grow on the nanotubes of cpTi, Ti6Al4V and Ti6Al4V-ELI. Titanium alloys with cells were permitted to incubate for 72 h. After incubation, the media was removed and cells were washed with HBSS (1×) (HyClone SH30588.01). Finally, the cells were fixed using 2.5% glutaraldehyde in PBS and placed in a refrigerator for 90 min. Samples were then taken out from the refrigerator and rinsed twice with HBSS. Afterwards, titanium alloys were dehydrated using 30%, 50%, 70%, 85% and 100% ethanol for 15 min. After dehydration, samples were placed in hexadimethylsilazane (HDMS) and allowed to dry over-night in the hood. The titanium specimens with cells were sputtered with gold for SEM analysis.

### 2.6. Cytotoxicity assessment

The effect of metal ions release from nanotubes on the cells was assessed by using MTS assay (G3580, Celltiter 96® AQueous One Solution Reagent, Promega Corporation) to determine the percent viability of MC3T3-E1 cells. cpTi, Ti6Al4V, and Ti6Al4V-ELI alloys were immersed in MEM alpha media for 15 days and the media were changed and collected after every 3 days. Cells were exposed to extracted media. The cells were cultured in MEM alpha media mixed with 10% FBS and 1% Penicillin–Streptomycin at 37 °C in a humidified atmosphere having 5% $CO_2$. Cells were counted ($2 \times 10^4$ cells) using a hemocytometer and plated in 96-well plates with 200 μl of culture media per well. The cells were incubated for 24 h to allow attachment. After the 24-hour incubation, the culture media were replaced with culture media exposed to titanium alloys. Pure culture media with cells were used as control. The cells were incubated for 24 h. After 24 h, 100 μl of media was removed from the 96-well plates, the remaining 100 μl media was treated with 20 μl/well with Celltiter 96® AQueous One Solution Reagent. The 96-well plates were placed in the incubator for 4 h. Immediately after the incubation period, the optical density measurements were recorded using ELx800™ BioTek absorbance microplate reader controlled by Gen5 software with a 490 nm absorbance excitation filter. Statistical analysis was executed to evaluate the difference in cell viability by the analysis of variance.

### 2.7. Statistical analysis

A one-way ANOVA analysis followed by post hoc testing (Tukey HSD) was performed on corrosion potential, corrosion rate, and MTS for cytotoxicity of cells by using ANOVA online calculator, (http://statpages.org/anova1sm.html). A significant difference between groups was interpreted to occur at $p < 0.05$. Sample sizes for these outcomes were as follows: (n = 3/group — Ecorr values; n = 3/group — Corrosion rates and n = 5 5/group for MTS data for cell viability per dosage of ionized media).

## 3. Results and discussion

### 3.1. Surface morphology and chemistry

The surface morphologies of the titanium alloys obtained after anodizing are witnessed under a scanning electron microscope as shown in Fig. 3. The micrographs clearly reveal that $TiO_2$ nanotubes are successfully grafted and aligned vertically. It can be seen that the nanotube array is uniform over the substrate.

In Fig. 3, the n1 shows the nanotubes grafted on the cpTi. These nanotubes are uniformly distributed on the surface of the substrate. The EDS analysis shows that these nanotubes have titanium and oxygen in higher concentration with small amounts of phosphorus. Phosphorus on the surface is from phosphoric acid present in the electrolyte (used during anodization). As the metallic surfaces are electropositive, the electronegative components in the electrolyte accumulate on the surface of the substrate. The presence of phosphate in nanotubes enhances the bioactivity, as phosphorus is one of the main constituents of bone. The nanotube on the cpTi alloy has a large diameter of about 100 nm in comparison with the nanotubes of Ti6Al4V and Ti6Al4V-ELI. In Fig. 3; n2 and n3 show nanotubes on Ti6Al4V and Ti6Al4V-ELI surfaces, respectively. The diameter of nanotubes on Ti6Al4V is smaller (70 nm) when compared with the diameter of nanotubes on Ti6Al4V-ELI (90 nm). It is interesting to note that each titanium alloy represents dissimilar densities of nanotubes. The smaller diameter of the nanotubes means higher density (number of nanotubes per unit area). The SEM micrographs depict that cpTi substrate has approximately 55 nanotubes per $\mu m^2$ of its area while the Ti6Al4V and Ti6Al4V-ELI have approximately 140 and 85 nanotubes per $\mu m^2$, respectively. The variation in the densities is current and voltage fluctuation assisted during the process of anodization and the etching of V-rich β phase in Ti6Al4V and Ti6Al4V-ELI [29]. During the electrochemical process the Beta phase suffers from complete dissolution during anodization. This behavior is also noticed in other electrolytes and is ascribed to the V-rich β phase dissolution and its passivity breakdown [30]. The etching of the V-rich β phase produces oxidized species in the electrolyte and the presence of fluoride in electrolyte is responsible for the current and voltage fluctuations [30]. As the nanotubular diameter is a function of anodization potential, thus the small fluctuation in current may alter the morphology of nanotubes [31]. This could be concluded that the pore wall separation is an obstacle if it comes to the quantitative description of the densities of the nanotubes on different titanium alloys.

From the EDS data, the nanotubes have titanium oxide with phosphate and fluoride. Both phosphate and fluoride are biocompatible and enhance the bioactivity of the material. When comparing the surface chemistry of each specimen, fluoride doesn't accumulate on cpTi as shown by EDS while Ti6Al4V and Ti6Al4V-ELI have fluoride on their surfaces.

### 3.2. Electrochemical analysis

#### 3.2.1. Cyclic potentiodynamic polarization

The metallic implants may be rejected due to corrosion in biological fluids if their surfaces are not modified to tolerate severe environment within the body. The aqueous medium of the human body consists of various ions such as chloride, phosphate, sodium, calcium and other low molecular species [32]. The biological fluids are buffered saline having a temperature of 37 °C and pH of 7.4 under normal conditions [33]. The metal ions release from the surface of implant may interact with biological environment and produce inflammatory reactions. This release of ions is a continuous process until the passive oxide film is regenerated. The decisive role of biological fluids and surface chemistry of implant

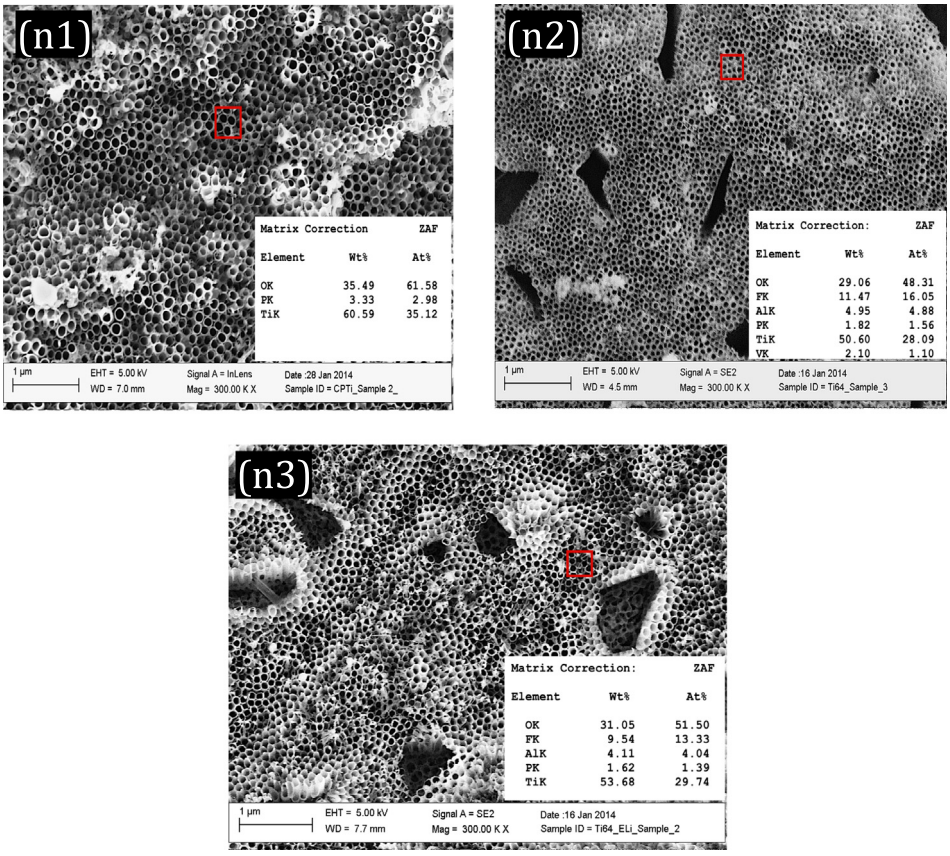


**Fig. 3.** SEM micrographs show the vertically aligned nanotubes on the surface of cpTi (n1), Ti6Al4V (n2) and Ti6Al4V-ELI (n3). Insets are EDS data showing the surface chemistry.

are critical aspects and may adversely affect the integrity and increase the chances of repetitive post operation surgeries [34].

The cyclic polarization scans as shown in Fig. 4 are obtained to evaluate passive behavior and localized corrosion tendency of anodized cpTi TNTs, Ti6Al4V TNTs and Ti6Al4V-ELI TNTs in phosphate buffer saline. During forward anodic polarization the slight increase in anodic current density depicts transient passive behavior due to ion transportation within the nanotubular structure at the surface of cpTi TNTs, Ti6Al4V TNTs and Ti6Al4V-ELI TNTs. The negative reverse polarization hysteresis also determines the resistance of these material surfaces towards localized dissolution.

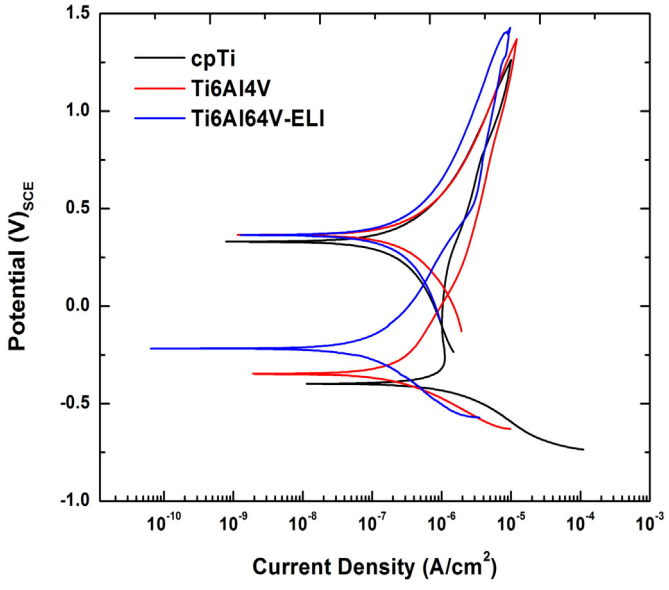


**Fig. 4.** Cyclic polarization scans in physiological body solution at 37 °C and 5% $CO_2$.

The slight difference in forward and reverse anodic polarization scans corresponds to the formation of barrier type nanoporous structure during anodization. The corrosion potential ($E_{corr}$) values of anodized cpTi TNTs, Ti6Al4V TNTs and Ti6Al4V-ELI TNTs having nanotubular structure are −357, −304 and −204 mV with respect to SCE, respectively. The relatively more negative (active) potential of anodized cpTi corresponds to higher corrosion susceptibility than titanium alloys. The least negative potential (−204 mV) exhibited by anodized Ti6Al4V-ELI TNTs assures its higher thermodynamic stability in physiological solution than Ti6Al4V TNTs and cpTi TNTs. The kinetic parameters determined by extrapolating the Tafel region of cyclic polarization scans (with standard deviations) are given in Table 2.

This also confirms that the corrosion current ($I_{corr}$) and hence corrosion rate of anodized Ti6Al4V-ELI are about 2.5 and 18 times lower than Ti6Al4V TNTs and cpTi TNTs respectively. Very low corrosion rate (0.025 mpy) of Ti6Al4V-ELI TNTs is attributed to formation of a high barrier type oxide film, which gives high resistance to dissolute in physiological solution. One-way ANOVA statistical analysis and post hoc Tukey HSD tests for the corrosion potentials of each alloy with grafted

**Table 2**
Quantitative data of cyclic polarization scans (n = 3).

| Sample | $E_{corr}$ (mV) | $I_{corr}$ (µA/cm$^2$) | $I_{pass}$ (µA/cm$^2$) | CR (mpy) |
|---|---|---|---|---|
| CPTi TNTs | −357 ± 40 | 1.340 ± 0.74 | 4.122 ± 0.4 | 0.467 ± 0.012 |
| Ti6Al4V TNTs | −304.7 ± 75 | 0.187 ± 0.25 | 3.373 ± 0.7 | 0.063 ± 0.006 |
| Ti6Al4V-ELI TNTs | −217.7 ± 10 | 0.075 ± 0.48 | 1.043 ± 0.5 | 0.025 ± 0.016 |

nanotubes demonstrate that there is a significant difference in the corrosion potential of the cpTi TNTs when compared to Ti6Al4V-ELI TNTs ($p < 0.05$) as shown in Fig. 5. Also the averaged passive current density ($I_{pass}$) of cpTi TNTs is found at 4.122 μA/cm$^2$, which is higher than the Ti6Al4V TNTs (3.373 μA/cm$^2$) and Ti6Al4V-ELI TNTs (1.043 μA/cm$^2$). This behavior shows the higher penetration of electrolyte in the nanotubular structure of cpTi and formation of galvanic cell due to lower barrier oxide film thickness at the bottom of the nanotube. Whereas the nano-patterned surface features on Ti6Al4V TNTs and Ti6Al4V-ELI TNTs restricted the dissolution of metal ions due to the formation of compact passive oxide pore wall [35]. Furthermore, the statistical analysis of corrosion rates of each nanotube has not shown any significant difference and $p > 0.05$ for the comparison in all groups of data. Fig. 6 shows the comparative variance in the corrosion rate of each anodized titanium alloy.

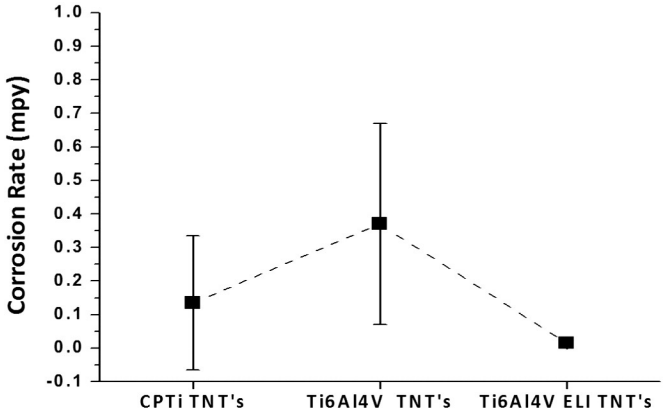


**Fig. 6.** Corrosion rates of alloys anodized for nanotubes for n = 3. The statistical analysis shows no significant difference in comparison of each group of data.

*3.2.2. Electrochemical impedance spectroscopy (EIS)*

Electrochemical impedance spectroscopy (EIS) is also used to determine the characteristics of oxide film produced over cpTi, Ti6Al4V, and Ti6Al4V-ELI through anodizing. This is an efficient technique to monitor kinetics of electrochemical reactions without changing the surface properties due to perturbation of small potential amplitude (10 mV rms) [36,37].

The Nyquist plots of anodized titanium alloys were obtained in PBS in a three-electrode cell assembly coupled with Gamry Potentiostat as shown in Fig. 7. To find the quantitative values of kinetic parameters involved during electrochemical contact of anodized surfaces with PBS, an equivalent electrical circuit (EEC) model is developed as depicted in Fig. 8. The simulated modeling results (with standard deviations) equivalent to EEC were obtained by fitting impedance spectra (Nyquist plots) and are displayed in Table 3.

The simulated EEC model consists of solution resistance ($R_s$) in series with a parallel circuit of constant phase element ($Y_o$) for development of non-ideal capacitance and charge transfer resistance (Rct). The inclusion of '$Y_o$' in EEC is due to the formation of non-homogeneous double layer by nanotubular structure. In low frequency regime of Nyquist spectrum of all anodized surfaces, a diffusional phenomenon is observed which may be due to the ingress of ionic species within the nanotubular structure of oxide film. This behavior is correlated with Warburg coefficient in series with Rct as shown in EEC. The non-uniform distribution of charge at the anodized surface of cpTi TNTs, Ti6Al4V TNTs and Ti6Al4V-ELI TNTs is evaluated by charge relaxation coefficient ($n < 1$) values in Table 4. The charge distribution characteristics of oxide film are found almost similar at all anodized cpTi TNT, Ti6Al4V TNT and Ti6Al4V-ELI TNT surfaces as there was a minor difference in the relaxation coefficient (n) values. But relatively high value of relaxation coefficient, 'n' (0.673) and lower constant phase element admittance '$Y_o$' (4.752 μS·sn/cm$^2$) of Ti6Al4V-ELI TNTs depicts lower charge dissipation in redox reactions due to good barrier characteristics of oxide film. But for other specimens i.e. Ti6Al4V TNTs and cpTi TNTs the slightly lower values of 'n' (0.661 & 0.659 respectively) and considerably higher '$Y_o$' correspond to lower restrictions of charge leakage through the non-uniform double layer at these surfaces. Furthermore, the improvement in the barrier properties of oxide film can be validated by the higher 'Rct' (177.6 kΩ·cm$^2$) of Ti6Al4V-ELI TNTs than Ti6Al4V TNTs and cpTi TNTs. The Warburg diffusional coefficient ($W_d$) represents the semi-infinite linear diffusion through the surface films. Moreover in our case it is related with the transport of ionic species in the electrolyte through the nanotubular structure. The admittance values (Wd) show the ease by which ions may approach the substrate and react. It is clear that the cpT TNTs showed higher diffusional characteristics (Wd = 141.3 μS·s$^{0.5}$/cm$^2$) than Ti6Al4V TNTs and Ti6Al4V-ELI TNTs. Even though there is slightly higher susceptibility of ion transportation on Ti6Al4V-ELI TNT (47.44 μS·s$^{0.5}$/cm$^2$) surface than Ti6Al4V TNTs (35.16 μS·s$^{0.5}$/cm$^2$) the risk of corrosion reactions is low due to higher charge transfer resistance of the barrier oxide layer at the bottom of the nanotubes. The EIS evaluations are in support of potentiodynamic cyclic polarization scan results and also validate the

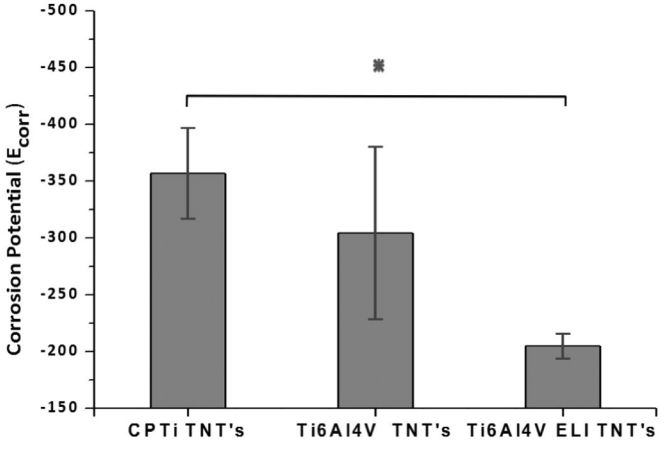


**Fig. 5.** The corrosion potentials (Ecorr) of each alloy with grafted nanotubes. For n = 3 ANOVA statistical analysis and post hoc Tukey HSD tests results demonstrate that there is significant difference of corrosion potential of the cpTi TNTs ($p < 0.05$) in comparison to Ti6Al4V-ELI TNTs.

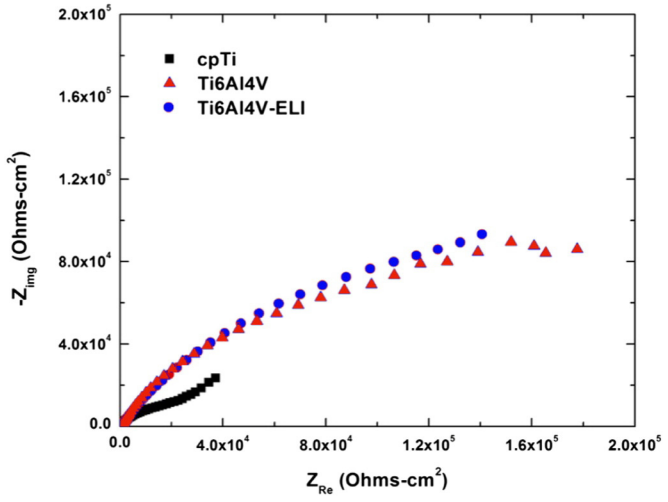


**Fig. 7.** EIS Nyquist plot of cpTi, Ti6Al4V and Ti6Al4V-ELI having nanotubes.

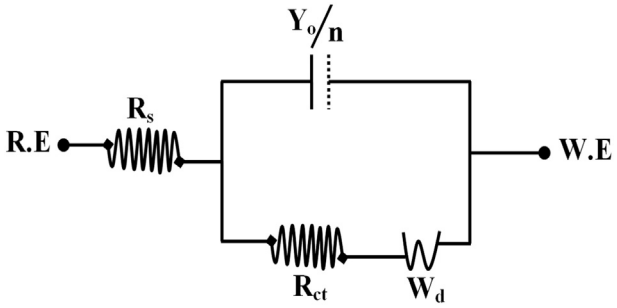


**Fig. 8.** Simulated equivalent circuit model for EIS spectrum of nanotubes on each specimen.

improvement in the corrosion resistance of Ti6Al4V-ELI TNTs by the formation of oxide film.

## 4. Cell adhesion study

Protein adsorption plays an important role in biomaterial–cell interaction. Changes in the surface chemistry and nanotopography can affect the protein adsorption characteristics. If the surface is porous and the size of asperities is larger than the protein dimension and chemically homogeneous then it will be more favorable for protein desorption and obviously cell proliferation. For the better understanding of cell–surface interaction on nano-scale, MC3T3 pre-osteoblast cells were allowed to proliferate on the nanotubes grafted on cpTi, Ti6Al4V and Ti6Al4V-ELI. The behavior of these alloys towards anodization was different as discussed above. The EDS data explicitly shows that the cpTi TNTs have phosphate on its surface while the Ti6Al4V TNTs and Ti6Al4V-ELI TNTs have different surface chemistry. On the other side the nanotubes of each sample show a difference in diameter although they all are anodized at the same condition, which provides different topographies for cell proliferation. These differences affect the cell morphology, organization and separation, which have direct effect on cell adhesion and osseointegration.

Normally the preosteoblast cells took 12 h to completely adhere on any surface. The adhesion starts from the extension of cell filopodia. These filopodia directly interact with the surface with the help of different types of proteins that's why the surface chemistry and topographic nature influence proliferation, cell differentiation rate and adhesion. Apparently the cell interaction to any surface at nanoscale seems similar to microscale. However, the cell attaches to the surface through discrete point attachments [16]. Several biological molecules are responsible for cell attachment but integrin plays a dominant role in the attachment process [38]. Integrins are transmembrane receptors that are the bridges for cell–cell and cell–extracellular matrix (ECM) interactions [39]. This allows rapid and flexible responses to events at the cell surface, e.g. to signal platelets to initiate an interaction with coagulation factors. Integrins have two subunits, α and β. During attachment process to any surface these subunits receptors cluster together and recruit other cytoplasmic proteins and form a complex called focal contact or focal adhesion as illustrated and is given in Fig. 9.

It has been observed that these focal contacts are less than 5 μm, super mature adhesion greater than 5 μm while integrins themselves are mobile at nanoscale [40]. These integrins are very sensitive to surface chemistry and surface topography which indicates great effect on cells at microscale. Furthermore, surface chemistry plays a dominant role at nanoscale. Surface chemistry is a deciding factor in determining which type of integrin is recruited by intermediacy of the absorbed proteins and thus affects focal adhesion. The nanoscale texture, pattern and chemistry have a significant impact on the organization and type of focal adhesion formed [41]. The focal adhesion is the process of inducing specific integrins, which are directly connected to the nucleus of the cell. Sometimes the cell needs to disrupt their formation to proliferate. During the process cell adhesion, the filopodia and lamellipodia worked as cell probes. These branch like structures probe the outside environment of the cell and their ends serve as hooks as shown in Fig. 9. As the nanotubes have tubular structure, it is likely that they will influence the cell growth. The tubular structure provides more space to absorb the cell protein and provides ledges for the cell filopodia to attach to the surface.

In our experimental study, the cells were incubated and fixed on the surface of each specimen. The explicit and significant cell morphological changes have been observed as shown in Fig. 10. In case of cpTi TNTs the cell proliferation is seem usual as clearly depicted in Fig. 10-a1 and -a2. The cells indicate healthy behavior and show much more pronounced protrusion of filopodia with significantly longer configuration and a high degree of contact as shown in Fig. 10-a2. The filopodia are also probing the surface and form more intimate contacts with the nanotubes. The interaction between the cell and the nanotubes allows for enhanced cellular propagation and an overall increase in cell–material interaction. The nanotubes may also facilitate movement because the tubular topography provides ledges. The pre-osteoblast cell after proliferation and adhesion shows nice extracellular interaction with the neighbor cells; by the support of filopodia through which the cell signal transduction takes place. The cells are spread with no preferential direction since they acquire a roughly flat form over the surface. Fig. 10-a1 and -b1 shows that the cell has normal cell adhesion showing large spread filopodia and small lamellipodia.

Fig. 10-b1 and -b2 depicts the pre osteoblast cell morphology on the Ti6Al4V TNTs. The cell proliferation on the surface appears typical but the cells have pores on the surface. These kinds of pores are common indication of cell apoptosis or necrosis but here this is not the case. To confirm this information, we had led our research to the cytotoxicity analysis of these nanotubes and cell viability study. This might have been due to the chemicals used during cell fixation. The cells spread in all direction and having flat morphology on the nanotubes. The pre-osteoblast cells on the surface of Ti6Al4V TNTs have noticeable protrusion but thinner filopodia in comparison with the cell morphology on cpTi TNTs. The ECM is improved and their network seems strong. The filopodia have no preferential direction. The filopodia are also probing the surface and form more intimate contacts with the nanotubes, sometimes protruding into the nanotube holes. The small particles between the cells are the ECM particles.

On the surface of the Ti6Al4V-ELI TNTs, pre-osteoblast cell morphology is depicted in Fig. 10-c1 and -c2. There is significant change in cell morphology in comparison with the cpTi TNTs and Ti6Al4V TNTs. Though the cells appear completely adhered to the nanotubes, there is no proper existence of the filopodia or the filopodia are very tiny, which is the source of the focal adhesion. It seems that the cell interacts with the surface by deforming its membrane [41]. This is due to the functioning of different processes which occur at the surface of the cells to regulate the important process inside the cell. Sometimes the

**Table 3**
Quantitative data of EIS measured and simulated with equivalent electric circuits (n = 3).

| Sample | $R_s$ ($\Omega \cdot cm^2$) | $R_{ct}$ ($k\Omega \cdot cm^2$) | $Y_o$ ($\mu S \cdot s^n/cm^2$) | n | $W_d$ ($\mu S \cdot s^{0.5}/cm^2$) |
|---|---|---|---|---|---|
| cpTi | 173.9 ± 8.1 | 37.11 ± 10.8 | 18.23 ± 0.11 | 0.659 ± 0.01 | 141.3 ± 6.3 |
| Ti6Al4V | 138.7 ± 7.8 | 140.7 ± 14.2 | 8.212 ± 0.13 | 0.661 ± 0.03 | 35.16 ± 5.6 |
| Ti6AL4V-ELI | 223.5 ± 13.6 | 177.6 ± 20.42 | 4.752 ± 0.22 | 0.673 ± 0.02 | 47.44 ± 3.8 |

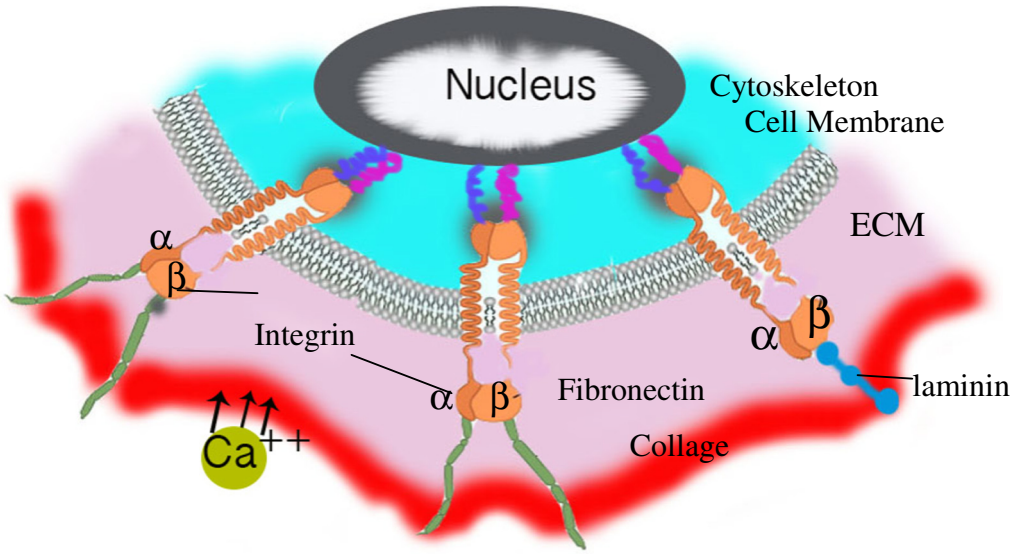


**Fig. 9.** A conceptual illustration of the cellular mechanical transduction mechanism. The signal transduction by the mechanical load or influx of ion (e.g. Ca ion) from ECM to integrin through the cytoskeleton to the nucleus results in the changes in the gene transcription and protein translation.

cells mechanically stretch to open the sacs to influx the ions and thus signaling in the nucleus takes place. These changes in the cell behavior in response to surface topography must be mediated by the transduction of the information to the nucleus. However the intracellular mechanisms by which this information is transmitted are not yet fully understood. In this present case the cell physiology shows that the extracellular matrix is influenced by surface chemistry or the size of the nanotubes. There is no communication between the cells and each cell is separated from the other.

The difference in surface structure (nanotubular width) and chemistry has an effect on the response of the preosteoblast cells on nanotube surfaces. The unique geometry of nanotube allows fluid spaces even after the cells cover the nanotube top surface, thus enabling a continued supply of natural fluids. Changes in the cell behavior in response to the surface topography are mediated by transduction of the information to the nucleus by direct or indirect mechanism. However, the intracellular transmissions of the signals through which the information are transmitted have not been fully understood. The elongation and the stretching of the cells can produce deformation in the nucleus, which influence the morphology and the behavior of the cell.

## 5. Biocompatibility analysis through cell viability

In order to investigate the effects of the leached ions from the nanotubes of each substrate on MC3T3 pre-osteoblast cells, cytotoxicity analysis was conducted. The activity was carried out for 15 days by exposing the calculated surface area to the culture media. The culture media, which was ionized by the immersion of each titanium alloy for different intervals were extracted. Afterwards pre-osteoblasts were allowed to grow in this media and the cell cytoscan-cytotoxicity MTS assay was conducted for each activity to inspect cell viability. The values of absorbance are converted to the bar plot as shown in Fig. 11. Each data is compared with the cell viability in the normal culture media as control.

The plots indicate that there is immediate decrease in MC3T3 preosteoblast cell viability in three days of ionized media in each case of substrate. Therefore the one-way Anova with post hoc Tukey test shows that there is significant difference in cell viability ($^{*}p < 0.05$). This substantial reduction of cell survival is due to the dissolution of the surface oxide layers having impurities and the extreme release of ions in the culture media during immersion [42,43]. Initially the ion dissolution is higher and reduces with time after repassivation in a specific environment. Though the specimens were cleaned and sonicated before exposing the media to the alloy in immersion test, the presence of dust particles on the surface, which couldn't be absolutely removed, could disturb the cell viability and impact its mortality. The extensive ion dissolution to the media, affects the cell organelles and their function.

The results show that cell survival became normalize after 3 days and cell viability with the 5 days ionized media shows improvement in the cell percent cell viability. The stabilization in viability might be due to reformation of the surface oxide film and the accumulations of salts from culture media on the surface of the specimens, which results in the reduction of the ion leakage to the media. From 7 to 15 days ionized media the Ti6Al4V TNTs show slight consistency while the cpTi TNTs and T6Al4V-ELI TNTs show constant cell viability.

In the case of cpTi TNTs there is substantial difference in cell survival of 10 days ($^{**}p < 0.05$) and 15 days ($^{***}p < 0.05$) in assessment with control media as shown in Fig. 11. Very low "p" value is investigated for 15 days media in comparison to other groups of cpTi TNTs. In case of the Ti6Al4V TNTs, as the significant reduction of cell survival is observed for 3 days media, the statistic shows the significant difference in comparison with control ($^{\circ}p < 0.05$). On the other side the Ti6Al4V TNTs show the noteworthy difference for 3 days media in comparison with 10 days ($\#\#p < 0.05$) and 15 days ($\#\#\#p < 0.05$).

The cyclic potentiodynamic scans and EIS evaluations are in support of percent cell viability scans and also validate the data. From the cyclic potentiodynamic scans, it is clear that the lowest Ecorr value was indicated by cpTi TNTs, followed by Ti6Al4V TNTs and than Ti6Al4V-ELI TNTs. Similarly, EIS of cpTi showed higher diffusional characteristics ($W_d = 141.3\ \mu S \cdot s^{0.5}/cm^2$) than Ti6Al4V TNTs and Ti6Al4V-ELI TNTs. This looks quite odd that the dissolution rate of cpTi TNTs is higher but the cell viability plot shows consistency in percent cell viability. The ions which leach from the cpTi to culture media per duration are less toxic in comparison. As we know that cpTi is 99.9% pure titanium, while Ti6Al4V TNTs and Ti6Al4V-ELI TNTs have aluminum and vanadium in them. This leaching of aluminum and vanadium may adversely affect the cell viability. Even though there is slightly higher susceptibility of ion transportation on the Ti6Al4V-ELI surface than Ti6Al4V TNTs, the risk of corrosion reactions is lower, due to higher charge transfer resistance of the barrier oxide layer at the bottom of the nanotubes. That is why the Ti6Al4V-ELI TNT ionized media are less toxic than Ti6Al4V TNTs and show stability in percent cell viability after 5 days media.

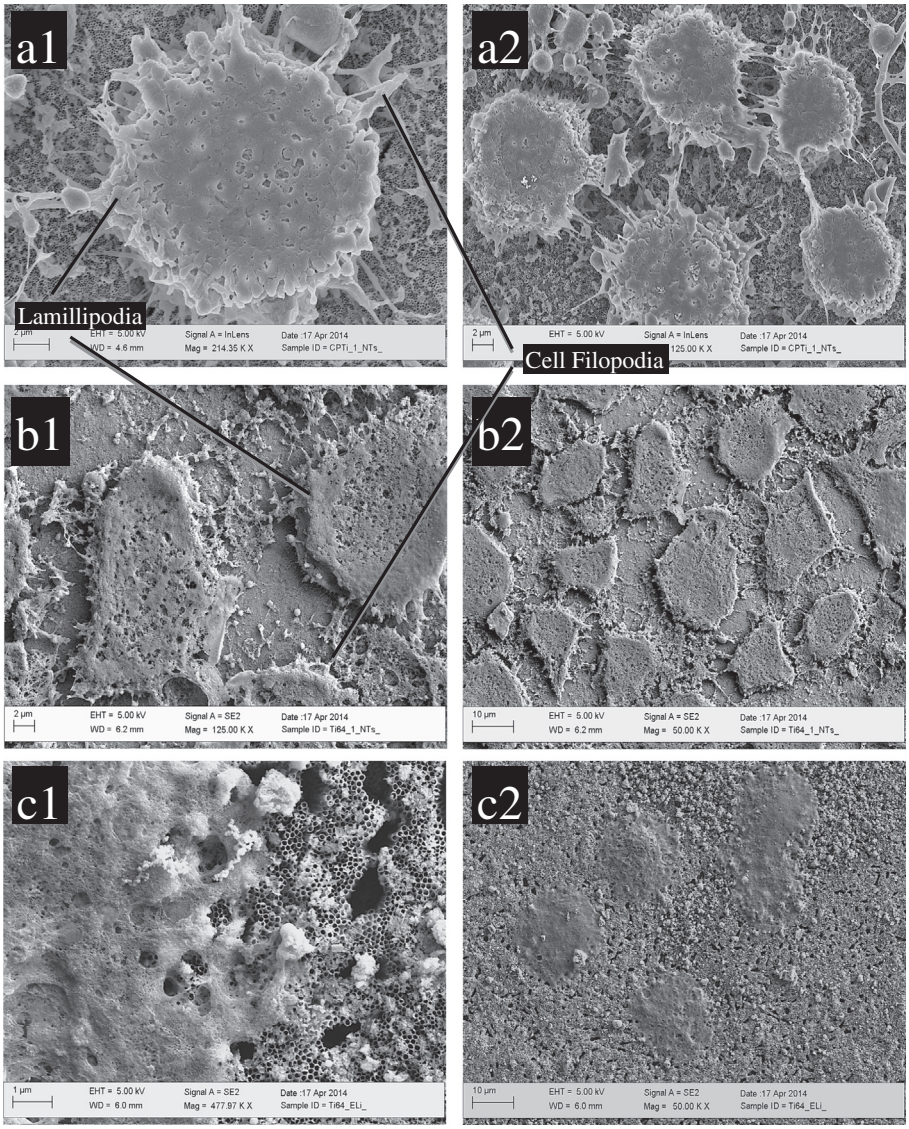


**Fig. 10.** SEM images of MC3T3 pre-osteoblast cells on the nanotubular surfaces for 3 days incubation. a1 & a2: CPTi TNTs; b1 & b2: Ti6Al4V TNTs; and c1 & c2: Ti6Al4V-ELI TNTs.

## 6. Conclusions

This study provides the synthesis and characterization that are necessary for successful applications of $TiO_2$ nanotubes for orthopedic applications. Self-organized $TiO_2$ nanotubes were grafted via simple anodization process on the surface of cpTi, Ti6Al4V and Ti6Al4V-ELI. The electrochemical analysis and biocompatibility studies indicate that passivation of the nanotubes has positive impact on the osteoblast cell viability. The nanotubes on the implant surface provide a powerful mechanism to encourage direct cell adhesion and proliferation by providing a better environment for typical migration processes. The nanotubes do not cause any adverse response to the pre-osteoblast cells. Thus, this research provides evidence that osteoblast cell activity can be significantly enhanced using controlled nanotopography. It is believed that continuing activity within this arena will hopefully bring new podium to improve osseointegration for orthopedic implants.

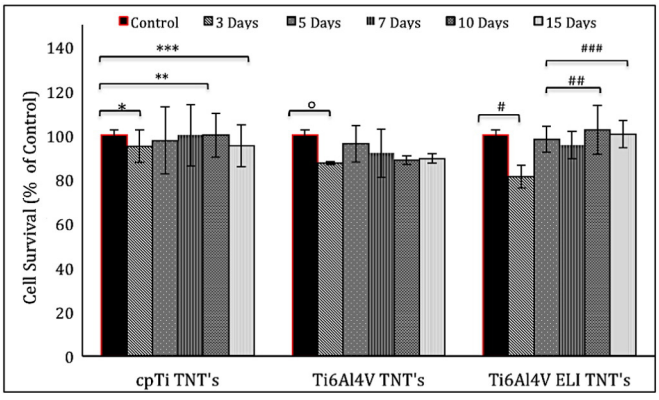


**Fig. 11.** Percent cell viability of preosteoblast cells in different concentrations of ions induces in-time and dose-dependent cytotoxic effects.

## Acknowledgment

The authors would like to acknowledge Ms. Estefania Gonzalez for the help with the anodization treatment.

## References

[1] C. Clifford, D. Hospital, Review Titanium: The Implant Material of Today, vol. 221987.

[2] H.J. Rack, J.I. Qazi, Titanium alloys for biomedical applications, Mater. Sci. Eng. C 26 (2006) 1269–1277.
[3] Waseem Haider, Enhanced biocompatibility of NiTi (nitinol) via surface treatment and alloying, FIU Electronic2010 (Theses and Dissertations, Paper 177).
[4] F. J. S., J. E. L., Buddy D. Ratner, Allan S. Hoffman, B.D. Ratner, A.S. Hoffman, F.J. Schoen, J.E. Lemons, Biomaterials science, An Introduction to Materials in Medicine, 3rd edition, Biomaterials Science: An Introduction to Materials in Medicine 2001, pp. 35–42.
[5] L. Trentani, F. Pelillo, F.C. Pavesi, L. Ceciliani, G. Cetta, A. Forlino, Evaluation of the TiMo 12 Zr 6 Fe 2 Alloy for Orthopaedic Implants: In Vitro Biocompatibility Study by Using Primary Human Fibroblasts and Osteoblasts, 23 (2002) 2863–2869.
[6] G.P. Kumar, L. Mathew, Self-expanding aortic valve stent-material optimization, Comput. Biol. Med. 42 (11) (Nov. 2012) 1060–1063.
[7] S. Bauer, P. Schmuki, K. von der Mark, J. Park, Engineering biocompatible implant surfaces, Prog. Mater. Sci. 58 (3) (Apr. 2013) 261–326.
[8] K.C. Popat, M. Eltgroth, T.J. LaTempa, C.A. Grimes, T.A. Desai, Decreased Staphylococcus epidermis adhesion and increased osteoblast functionality on antibiotic-loaded titania nanotubes, Biomaterials 28 (2007) 4880–4888.
[9] T.J. Webster, C. Ergun, R.H. Doremus, R.W. Siegel, R. Bizios, Enhanced functions of osteoblasts on nanophase ceramics, Biomaterials 21 (2000) 1803–1810.
[10] R.T. Beck, K.D. Illingworth, K.J. Saleh, Review of periprosthetic osteolysis in total joint arthroplasty: an emphasis on host factors and future directions, J. Orthop. Res. 30 (2012) 541–546.
[11] W. Weng, J.L. Baptista, Sol–gel derived porous hydroxyapatite coatings, J. Mater. Sci. Mater. Med. 9 (1998) 159–163.
[12] S. Oh, C. Daraio, L.-H. Chen, T.R. Pisanic, R.R. Fiñones, S. Jin, Significantly accelerated osteoblast cell growth on aligned TiO2 nanotubes, J. Biomed. Mater. Res. A 78 (2006) 97–103.
[13] D. Qiu, A. Wang, Y. Yin, Characterization and corrosion behavior of hydroxyapatite/zirconia composite coating on NiTi fabricated by electrochemical deposition, Appl. Surf. Sci. 257 (2010) 1774–1778.
[14] T. Zhao, Y. Li, X. Zhao, H. Chen, T. Zhang, Ni ion release, osteoblast–material interactions, and hemocompatibility of hafnium-implanted NiTi alloy, J. Biomed. Mater. Res. B Appl. Biomater. 100 (3) (Apr. 2012) 646–659.
[15] D. Persaud-Sharma, N. Munroe, A. McGoron, Electro and magneto-electropolished surface micro-patterning on binary and ternary nitinol, Trends Biomater. Artif. Organs 26 (2) (Jan. 2012) 74–85.
[16] K. Anselme, Osteoblast adhesion on biomaterials, Biomaterials 21 (2000) 667–681.
[17] B.D. Boyan, T.W. Hummert, D.D. Dean, Z. Schwartz, Role of material surfaces in regulating bone and cartilage cell response, Biomaterials 17 (1996) 137–146.
[18] K. Kieswetter, Z. Schwartz, T.W. Hummert, D.L. Cochran, J. Simpson, D.D. Dean, B.D. Boyan, Surface roughness modulates the local production of growth factors and cytokines by osteoblast-like MG-63 cells, J. Biomed. Mater. Res. 32 (1996) 55–63.
[19] B. Feng, J.Y. Chen, S.K. Qi, L. He, J.Z. Zhao, X.D. Zhang, Characterization of surface oxide films on titanium and bioactivity, J. Mater. Sci. Mater. Med. 13 (2002) 457–464.
[20] J.E. Feighan, V.M. Goldberg, D. Davy, J.A. Parr, S. Stevenson, The influence of surface-blasting on the incorporation of titanium-alloy implants in a rabbit intramedullary model, J. Bone Joint Surg. Am. 77 (1995) 1380–1395.
[21] S.F. Hulbert, S.J. Morrison, J.J. Klawitter, Tissue reaction to three ceramics of porous and non-porous structures, J. Biomed. Mater. Res. 6 (1972) 347–374.
[22] R. Zhou, D. Wei, H. Yang, W. Feng, S. Cheng, B. Li, Y. Wang, D. Jia, Y. Zhou, MC3T3-E1 cell response of amorphous phase/TiO2 nanocrystal composite coating prepared by microarc oxidation on titanium, Mater. Sci. Eng. C 39 (Jun. 2014) 186–195.
[23] D.S. Hwang, S.B. Sim, H.J. Cha, Cell adhesion biomaterial based on mussel adhesive protein fused with RGD peptide, Biomaterials 28 (2007) 4039–4046.
[24] D.A. Puleo, A. Nanci, Understanding and controlling the bone–implant interface, Biomaterials 20 (1999) 2311–2321.
[25] I. Degasne, M.F. Baslé, V. Demais, G. Huré, M. Lesourd, B. Grolleau, L. Mercier, D. Chappard, Effects of roughness, fibronectin and vitronectin on attachment, spreading, and proliferation of human osteoblast-like cells (Saos-2) on titanium surfaces, Calcif. Tissue Int. 64 (6) (Jun. 1999) 499–507.
[26] K.C. Popat, L. Leoni, C.A. Grimes, T.A. Desai, Influence of engineered titania nanotubular surfaces on bone cells, Biomaterials 28 (21) (Jul. 2007) 3188–3197.
[27] M. Wang, N.J. Castro, J. Li, M. Keidar, L.G. Zhang, Greater osteoblast and mesenchymal stem cell adhesion and proliferation on titanium with hydrothermally treated nanocrystalline hydroxyapatite/magnetically treated carbon nanotubes, J. Nanosci. Nanotechnol. 12 (2012) 7692–7702.
[28] K.M. Deen, A. Farooq, M.A. Raza, W. Haider, Effect of electrolyte composition on $TiO_2$ nanotubular structure formation and its electrochemical evaluation, Electrochim. Acta 117 (2014) 329–335.
[29] J.M. Macak, H. Tsuchiya, L. Taveira, A. Ghicov, P. Schmuki, Self-organized nanotubular oxide layers on Ti-6Al-7Nb and Ti-6Al-4V formed by anodization in NH4F solutions, J. Biomed. Mater. Res. Part A 75 (4) (2005) 928–933.
[30] K. Lee, H. Choe, Y. Ko, W. a Brantley, Nanotubular Structure Formation on Ti-6Al-4V and Ti–Ta Alloy Surfaces by Electrochemical Methods, vol. 50, no. 22012 164–170.
[31] S.K. Mohapatra, K.S. Raja, M. Misra, V.K. Mahajan, M. Ahmadian, Synthesis of self-organized mixed oxide nanotubes by sonoelectrochemical anodization of Ti–8Mn alloy, Electrochim. Acta 53 (2) (2007) 590–597.
[32] G. Manivasagam, D. Dhinasekaran, and A. Rajamanickam, "Biomedical Implants: Corrosion and its Prevention - A Review ~ !2009-12-22 ~ !2010-01-20 ~ !2010-05-25 ~ !", Recent Patents on, Corros. Sci., vol. 2. pp. 40–54, 2010.
[33] A. Oyane, H.-M. Kim, T. Furuya, T. Kokubo, T. Miyazaki, T. Nakamura, Preparation and assessment of revised simulated body fluids, J. Biomed. Mater. Res. A 65 (2003) 188–195.
[34] M.A. Khan, R.L. Williams, D.F. Williams, In-vitro corrosion and wear of titanium alloys in the biological environment, Biomaterials 17 (1996) 2117–2126.
[35] J. Baszkiewicz, D. Krupa, J. Mizera, J.W.W. Sobczak, A. Bilinski, A. Biliński, Corrosion resistance of the surface layers formed on titanium by plasma electrolytic oxidation and hydrothermal treatment, Vacuum 78 (2005) 143–147.
[36] M.E.P. Souza, M. Ballester, C.M.A. Freire, EIS characterisation of Ti anodic oxide porous films formed using modulated potential, Surf. Coat. Technol. 201 (2007) 7775–7780.
[37] K.M. Deen, A. Farooq, M.A. Raza, R. Ahmad, W. Haider, Estimating the degradation of methylethionium chloride dye on nanotubular TiO2 structure, J. Ind. Eng. Chem. 22 (2015) 153–158.
[38] U. Hersel, C. Dahmen, H. Kessler, RGD modified polymers: biomaterials for stimulated cell adhesion and beyond, Biomaterials 24 (2003) 4385–4415.
[39] J.-P. Xiong, Crystal structure of the extracellular segment of integrin alpha Vbeta 3, Science 294 (2001) 339–345.
[40] E.A. Cavalcanti-Adam, A. Micoulet, J. Blümmel, J. Auernheimer, H. Kessler, J.P. Spatz, Lateral spacing of integrin ligands influences cell spreading and focal adhesion assembly, Eur. J. Cell Biol. 85 (2006) 219–224.
[41] K. Anselme, P. Davidson, A.M. Popa, M. Giazzon, M. Liley, L. Ploux, The interaction of cells and bacteria with surfaces structured at the nanometre scale, Acta Biomater. 6 (2010) 3824–3846.
[42] C. Pulletikurthi, N. Munroe, D. Stewart, W. Haider, S. Amruthaluri, R. Rokicki, M. Dugrot, S. Ramaswamy, Utility of magneto-electropolished ternary nitinol alloys for blood-contacting applications, J. Biomed. Mater. Res. B Appl. Biomater. (2014)http://dx.doi.org/10.1002/jbm.b.33317.
[43] M. Rizwan, A. Ahmad, K.M. Deen, W. Haider, Electrochemical behavior and biological response of mesenchymal stem cells on cp-Ti after N-ions implantation, Appl. Surf. Sci. 320 (2014) 718–724.